

## Article

# Spatiotemporal Dynamics and Driving Factors of Soil Salinization: A Case Study of the Yutian Oasis, Xinjiang, China

Shiqin Li <sup>1,2</sup>, Ilyas Nurmemet <sup>1,2,\*</sup> , Jumeniyaz Seydehmet <sup>3,4</sup>, Xiaobo Lv <sup>1,2</sup>, Yilizhati Aili <sup>1,2</sup> and Xinru Yu <sup>1,2</sup>

<sup>1</sup> College of Geography and Remote Sensing Sciences, Xinjiang University, Urumqi 830046, China; 107552203693@stu.xju.edu.cn (S.L.); 107552201156@stu.xju.edu.cn (X.L.); 107552201173@stu.xju.edu.cn (Y.A.); 107552201175@stu.xju.edu.cn (X.Y.)

<sup>2</sup> Xinjiang Key Laboratory of Oasis Ecology, Xinjiang University, Urumqi 830046, China

<sup>3</sup> College of Geographical Science and Tourism, Xinjiang Normal University, Urumqi 830017, China; jumeniyaz@xjnu.edu.cn

<sup>4</sup> Xinjiang Laboratory of Lake Environment and Resources in Arid Zone, Xinjiang Normal University, Urumqi 830017, China

\* Correspondence: ilyas@xju.edu.cn

**Abstract:** Soil salinization is a critical global environmental issue, exacerbated by climatic and anthropogenic factors, and posing significant threats to agricultural productivity and ecological stability in arid regions. Therefore, remote sensing-based dynamic monitoring of soil salinization is crucial for timely assessment and effective mitigation strategies. This study used Landsat imagery from 2001 to 2021 to evaluate the potential of support vector machine (SVM) and classification and regression tree (CART) models for monitoring soil salinization, enabling the spatiotemporal mapping of soil salinity in the Yutian Oasis. In addition, the land use transfer matrix and spatial overlay analysis were employed to comprehensively analyze the spatiotemporal trends of soil salinization. The geographical detector (Geo Detector) tool was used to explore the driving factors of the spatiotemporal evolution of salinization. The results indicated that the CART model achieved 5.3% higher classification accuracy than the SVM, effectively mapping the distribution of soil salinization and showing a 26.76% decrease in salinized areas from 2001 to 2021. Improvements in secondary salinization and increased vegetation coverage were the primary contributors to this reduction. Geo Detector analysis highlighted vegetation (NDVI) as the dominant factor, and its interaction with soil moisture (NDWI) has a significant impact on the spatial and temporal distribution of soil salinity. This study provides a robust method for monitoring soil salinization, offering critical insights for effective salinization management and sustainable agricultural practices in arid regions.

**Keywords:** CART; geographical detector; soil salinization mapping; spatiotemporal variation; spatiotemporal distribution



**Citation:** Li, S.; Nurmemet, I.; Seydehmet, J.; Lv, X.; Aili, Y.; Yu, X. Spatiotemporal Dynamics and Driving Factors of Soil Salinization: A Case Study of the Yutian Oasis, Xinjiang, China. *Land* **2024**, *13*, 1941. <https://doi.org/10.3390/land13111941>

Academic Editor: Paolo Nasta

Received: 29 October 2024

Revised: 12 November 2024

Accepted: 14 November 2024

Published: 18 November 2024



**Copyright:** © 2024 by the authors. Licensee MDPI, Basel, Switzerland. This article is an open access article distributed under the terms and conditions of the Creative Commons Attribution (CC BY) license (<https://creativecommons.org/licenses/by/4.0/>).

## 1. Introduction

Soil salinization, a type of soil degradation, is one of the most critical and widespread environmental issues globally in arid and semi-arid regions [1]. Approximately one billion hectares of land are affected by salinization worldwide, accounting for 7% of the total land area. In arid and semi-arid regions, factors such as low rainfall, high evaporation rates, elevated groundwater levels, and high concentrations of soluble salts exacerbate the issue of soil salinization [2]. Soil salinization not only hinders local agricultural productivity and sustainable economic development but also contributes to the ecological degradation of oases in arid regions [3,4]. Thus, dynamic monitoring of soil salinization is essential for mitigating its impacts and serves as a scientific foundation for improving and utilizing saline soils.

Soil salinization mapping is an effective method for acquiring and expressing spatial distribution information of soil salinity to achieve dynamic monitoring of salinization [5].

Traditionally, large-scale and detailed digital soil salinization maps have been generated through field surveys and sampling, which are time-consuming and labor-intensive, limiting the feasibility of mapping and monitoring over large areas [6]. The advent of remote sensing technology has provided a rapid and efficient scientific method for mapping soil salinization [7].

In recent years, with the advancement of research [8], a more systematic theoretical framework has emerged, covering the distribution of saline soils, the characteristics of salinization [9], and the mechanisms and trends of its evolution [10,11]. Previous studies primarily focused on utilizing spectral information to construct inversion models, which have become a crucial approach for digital soil salinization mapping [12,13]. This highlights the great potential and efficiency of remote sensing technology in soil salinization monitoring. With the maturation of machine learning algorithms, their application in spatiotemporal soil salinization mapping and digital cartography has demonstrated significant potential [14,15]. Integrating remote sensing data with machine learning enables the construction of a more robust analytical framework [7], efficiently handling large-scale datasets and feature sets, ultimately producing higher-precision digital soil salinization maps [16,17].

However, previous studies have often relied on single-temporal remote sensing data, which lacks comprehensive analysis of the spatiotemporal characteristics of soil salinization. Over time, soil salinity redistributes within the soil, making salinization a dynamic process, that leads to changes in the spatiotemporal distribution and degree of salinization [18]. The use of multi-temporal remote sensing imagery to monitor and assess dynamic salinity changes can more comprehensively capture the temporal trends of salinization and its evolutionary processes, while mitigating the impacts of spectral confusion, such as “same spectrum, different objects” and “same object, different spectra” [19]. Various scholars have conducted dynamic monitoring studies of soil salinization in diverse geographical environments, such as oases [20], grasslands [21], river deltas [22], coastal plains [23], and farmlands [24]. These studies have successfully produced spatiotemporal maps of salinization that reveal its trends and distribution patterns. Such research demonstrates the feasibility of combining satellite imagery with spatiotemporal analysis for monitoring and assessing regional salinization dynamics [25], providing important scientific foundations for regional resource management and utilization.

Time-series monitoring of soil salinization heavily relies on remote sensing data and field measurements. However, due to technological limitations, high costs, and incomplete methodologies, current data are insufficient to support long-term time-series mapping of soil salinization. Moreover, significant variations in soil spectral characteristics, caused by different sources and types of salinity [26], make it challenging to develop a universal time-series inversion model for soil salinity. Therefore, in the absence of sufficient data, qualitative research based on expert interpretation, field databases, and salinization characteristics offers more advantages than quantitative studies at a temporal scale.

As research on soil salinization deepens, scholars have begun to focus on the driving factors behind its changes. Spatial information science and geostatistical methods have proven to be effective tools for dynamically monitoring salinization. Several studies [27–30] have employed the Geo Detector [31] to analyze the dominant factors and driving forces of soil salinization, contributing to a better understanding of the salinization process and its dynamic changes.

Therefore, the integration of remote sensing and geographic information science enables rapid, large-scale dynamic monitoring of saline land and the acquisition of temporal evolution data, which are crucial for assessing soil improvement as well as the sustainable development and utilization of land [32]. This study aims to utilize remote sensing imagery and machine learning classification algorithms to analyze the spatiotemporal distribution characteristics and trends of soil salinization in the Yutian Oasis and to investigate the driving factors behind these changes. The findings will play a critical role in stabilizing the local ecological environment and ensuring sustainable agricultural production in the

oasis, providing valuable scientific insights for the improvement, utilization, and ecological restoration of saline soils.

## 2. Materials and Methods

### 2.1. Study Area

As shown in Figure 1. Yutian County is located in the southern part of Xinjiang Uygur Autonomous Region, China (81°9′–82°51′ E, 35°14′–39°29′ N). The region experiences a typical temperate arid desert climate with an average annual temperature of 11.6 °C [33]. The extreme maximum temperature can reach 43 °C. The region’s average annual evaporation is 1708.49 mm, and the average annual precipitation is 55.87 mm. The average annual water resources total  $4.2 \times 10^9$  m<sup>3</sup>, of which 32.4% is available for use. Surface water accounts for 20%, while groundwater accounts for 12.4% of the total water resources [34]. Due to the intense surface evapotranspiration, the problems of soil salinization and desertification in the plain and desert areas have become increasingly severe. The salinized soils are primarily distributed in the transitional zones in the central region of the Yutian Oasis and in the desert-saline soil interlaced zones in the northern part of the oasis, where evapotranspiration is intense [35].

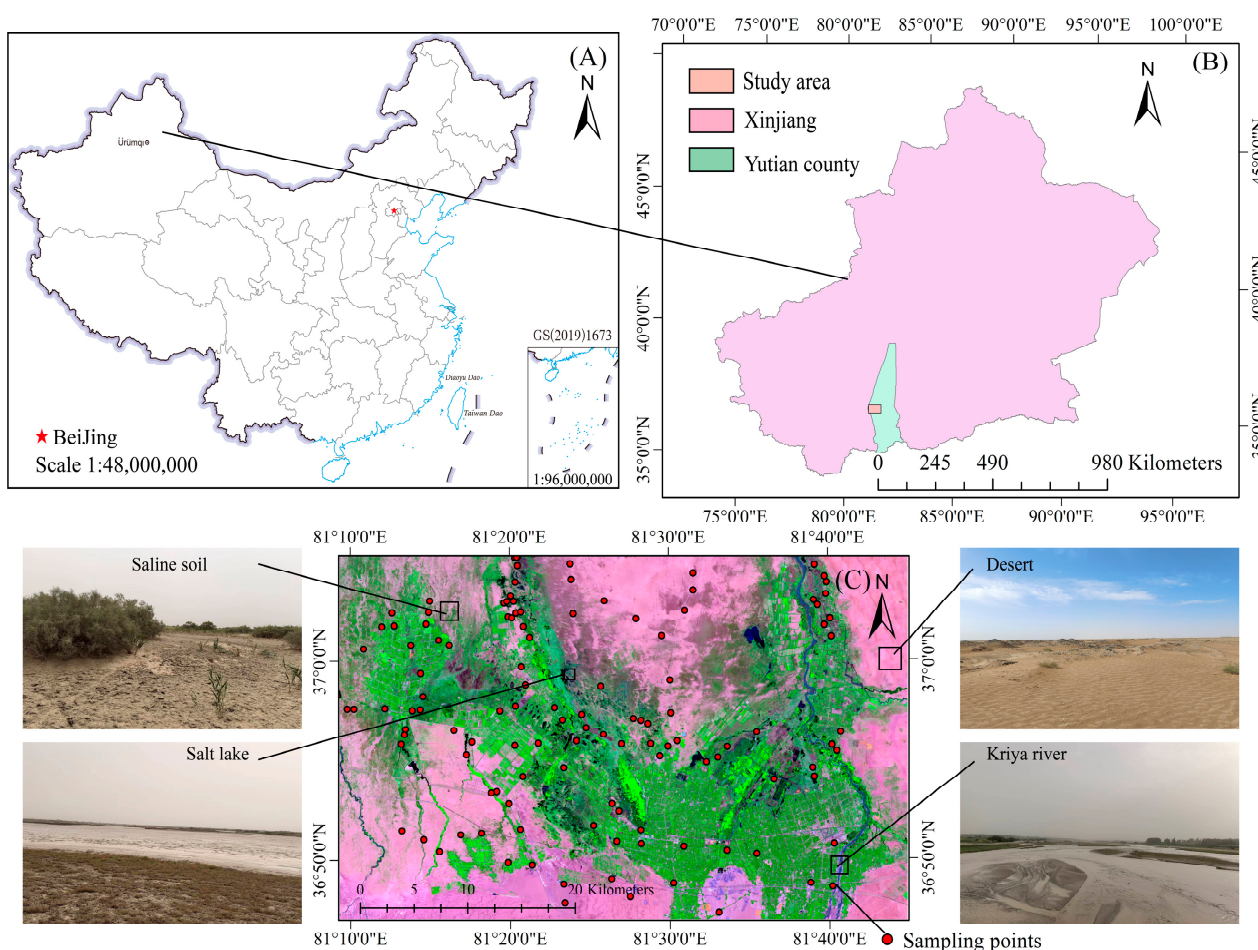


**Figure 1.** Overview of the study area. (A) Map of China. (B) Map of Xinjiang, China, Yutian County, and study area. (C) Map of the study area. Figure (C) shows Landsat8 OLI 15 July 2021 remote sensing image of the study area.

### 2.2. Remote Sensing Data Sources and Soil Sample Data

The Landsat remote sensing imagery used in this study was obtained from the open-source data platform Earth Explorer (<https://earthexplorer.usgs.gov/> accessed on 25 October 2024), with the data classified as Collection 2 Level 1. Given the distinct dry and wet

seasons in the study area, to minimize the influence of climate and seasonal factors on soil salinization mapping [36], cloud-free Landsat images of the study area were selected. The timeframe was restricted to the dry season, specifically from June to August. The detailed satellite imagery parameters are provided in Table 1.

**Table 1.** Data source.

Image Collection	Time	Resolution
Landsat7 ETM+	30 June 2001	30 m
Landsat5 TM	22 July 2006	
Landsat 5 TM	5 August 2011	
Landsat8 OLI	15 June 2016	
Landsat8 OLI	15 July 2021	

Based on different land use patterns, vegetation types, and soil characteristics in the Yutian Oasis, we established 140 typical sample points in the study area. Soil samples were collected using the three-point method and subsequently brought to the laboratory. Representative salinity indicators or parameters, including pH value, salinity, and electrical conductivity (EC) [37] of a saturated soil paste extract, were measured using a conductivity meter and pH meter.

### 2.3. Workflow

The workflow used in this study is shown in Figure 2. Initially, Landsat remote sensing images were preprocessed, including radiometric calibration, atmospheric correction, geographic registration, and image cropping. Spectral features and parameters were then extracted from multi-temporal images, creating a dataset of driving factors. The 420 field samples were divided into training (70%) and validation (30%) sets, consisting of 140 saline soil samples and 280 samples of vegetation, water bodies, deserts, buildings, and bare land. Soil salinization was classified using SVM and CART models, with accuracy assessed through confusion matrices and field data. The best-performing model was used to produce spatiotemporal maps of soil salinization. Finally, land use transfer matrices and spatial overlay analysis were employed to study salinization transitions and evolution, with the Geo Detector tool identifying the driving factors of these changes.



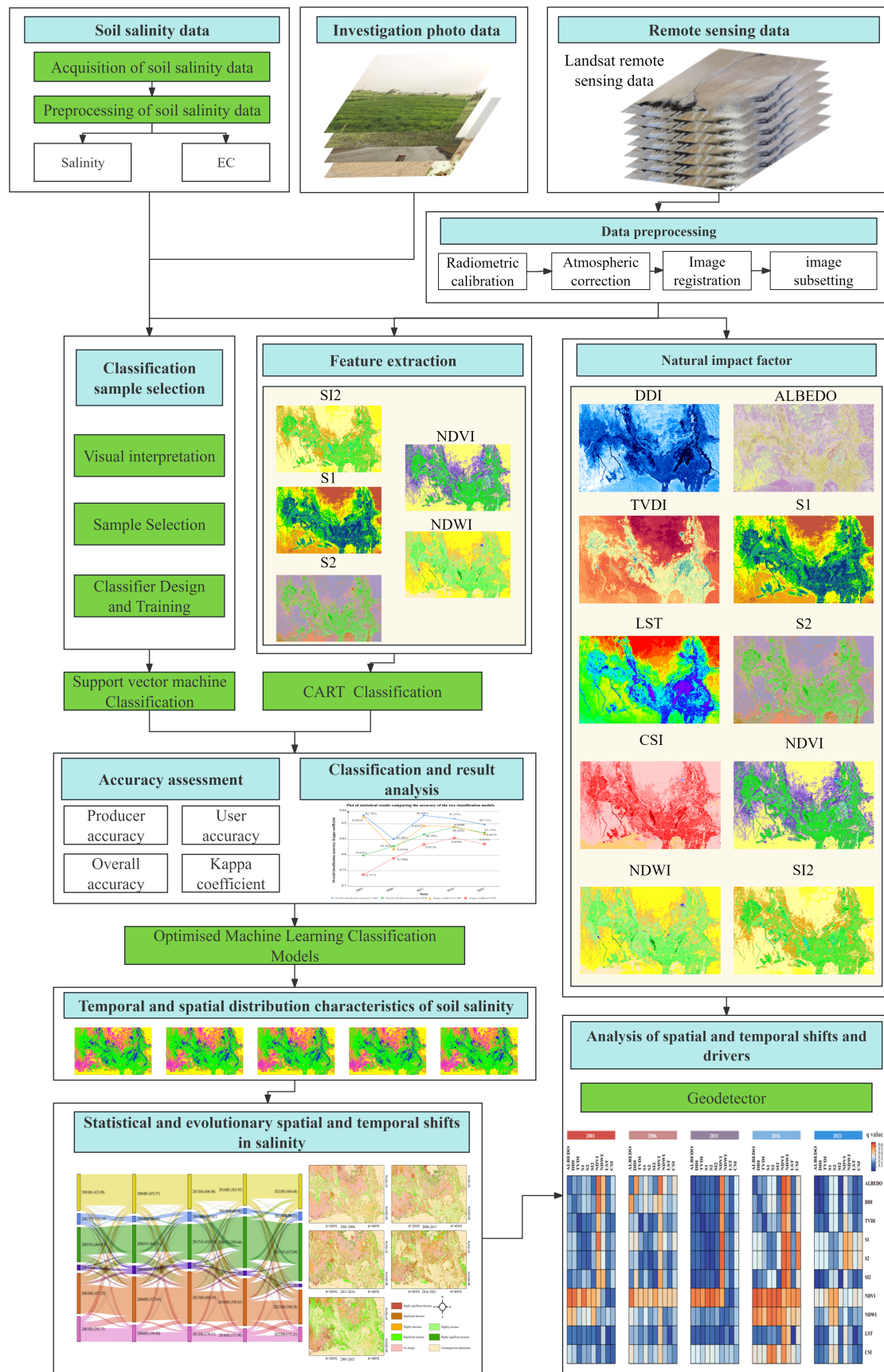


Figure 2. Workflow.

### 2.4. Feature Extraction

To minimize noise interference from the raw images and to better extract and differentiate soil with varying degrees of salinization, this study selected spectral indices [5,38,39] that have significant correlations with saline soils, based on previous research findings. These spectral indices were used as the spectral feature set for the CART classification. The specific inversion formulas and references for the spectral indices are shown in Table 2.

**Table 2.** Formula and reference of the spectral features.

Index	Calculation Methods	Reference
Spectral features for classification		
Normalized Difference Vegetation Index NDVI	$NDVI = (\rho_{NIR} - \rho_{Red}) / (\rho_{NIR} + \rho_{Red})$	[40]
Normalized Difference Water Index NDWI	$NDWI = (\rho_{Green} - \rho_{NIR}) / (\rho_{NIR} + \rho_{Green})$	[41]
Salinity Index 1 S1	$S_1 = \rho_{Blue} / \rho_{Red}$	[39]
Salinity Index 2 S2	$S_2 = (\rho_{Blue} - \rho_{Red}) / (\rho_{Blue} + \rho_{Red})$	[39]
Salinity Index SI2	$SI2 = \sqrt{\rho_{Green}^2 + \rho_{Red}^2 + \rho_{NIR}^2}$	[42]
Driving factor		
Salinity Index SI-T	$SI - T = (\rho_{Red} / \rho_{NIR}) \times 100$	[43]
Salinity Index SI1	$SI1 = \sqrt{\rho_{Green} \times \rho_{Red}}$	[42]
Normalized Difference Salinity Index NDSI	$NDSI = (\rho_{Red} - \rho_{NIR}) / (\rho_{NIR} + \rho_{Red})$	[44]
Comprehensive Salinity Index CSI	$CSI = \frac{NDSI + S_2 + SI - T}{3}$	
Land Surface Temperature LST	$LST = \frac{K_2}{\left(\ln \frac{K_1}{B(T_s)} + 1\right)}$	
	TM $\rho_{thermal1}$ $K_1 = 607.76 \text{ W/m}^2 \times \mu\text{m} \times sr, K_2 = 1260.56 \text{ K}$	[45]
	ETM+ $\rho_{thermal1}$ $K_1 = 666.09 \text{ W/m}^2 \times \mu\text{m} \times sr, K_2 = 1282.71 \text{ K}$	[46]
	TIRS $\rho_{thermal1}$ $K_1 = 774.89 \text{ W/m}^2 \times \mu\text{m} \times sr, K_2 = 1321.08 \text{ K}$	[47]
$K_1$ and $K_2$ as Calibration Conversion Parameters for Landsat Satellites, and $B(T_s)$ as Radiance, Calculable via the USGS Website.		
Albedo	$Albedo = 0.356 \times \rho_{Blue} + 0.130 \times \rho_{Red} + 0.373 \times \rho_{NIR} + 0.085 \times \rho_{SWIR1} + 0.072 \times \rho_{SWIR2} - 0.0018$	[48]
Desertification Difference Index DDI	$DDI = a \times NDVI - Albedo$ a is the intercept of the linear fit of NDVI and Albedo	[49]
Temperature Vegetation Drought Index TVDI	$TVDI = \frac{T_s - T_{Smin}}{T_{Smax} - T_{Smin}}$ $T_{Smax} = a_1 + b_1 \times NDVI$ $T_{Smin} = a_1 + b_1 \times NDVI$ $T_s$ represents the land surface temperature (LST), and $T_{Smax}$ is the maximum surface temperature for a specific NDVI value, representing the "dry edge". $T_{Smin}$ is the minimum surface temperature for a specific NDVI value, representing the "wet edge"	[50]
Annotation	$\rho_{Blue}, \rho_{Green}, \rho_{Red}, \rho_{NIR}, \rho_{SWIR1}, \rho_{SWIR2}, \rho_{Thermal}$ correspond to the blue, green, red, near-infrared 1, near-infrared 2, and thermal infrared bands of the Landsat satellite.	

Additionally, to identify the driving factors behind the soil salinization dynamics in the Yutian Oasis, this study extracted remote sensing indices such as albedo, DDI, TVDI, and LST based on previous studies, to analyze the driving factors of the spatiotemporal evolution of soil salinization.

In which the comprehensive salinity index (CSI) [38] was derived based on previous research findings as a relevant salinity index. Selecting three salinity indices with strong correlations. These three indices were normalized, and equal weights were assigned to represent the salinity levels in the study area.

The specific calculation methods and inversion formulas are provided in Table 2.

2.5. Soil Salinization Mapping and Classification Methods

2.5.1. Soil Salinity Classification Criteria and Classification Systems

Based on previous studies [51], saline soils were classified into three categories, as shown in Table 3. Using our soil sampling data, the classification standards were combined with visual interpretation standards to establish the following soil salinization classification system.

Table 3. Classification criteria and characterization.







Ec (dS/m)	Classification	Surface Feature Characterization	Landscape
Non-salinization	Water body	Salt lakes, rivers, reservoirs, wetlands	
	Bare land, desert, and building	Desert, bare land, buildings, wasteland, gobi	
	Vegetation	High vegetation coverage, farmland, orchard inter-planting	
2–4	Low salinization	Growing degraded plants, low shrubs, and drought-tolerant vegetation, 10–20% vegetation coverage, salt crust not obvious	
4–8	Moderately salinization	Mixed white spots, 5–10% vegetation coverage, brownish-white banding, thin salt crust visible	

Table 3. Cont.

Ec (dS/m)	Classification	Surface Feature Characterization	Landscape
>8	Highly salinization	0–5% vegetation coverage, white patches, clear salt spots, and salt crust	

### 2.5.2. Support Vector Machine (SVM)

SVM is renowned for its strong generalization ability and robustness with small sample datasets, making it particularly suitable for handling complex remote sensing image classification problems [52], and has been widely applied in remote sensing image classification. In this study, SVM was used to extract soil salinization information, with a focus on model type and parameter selection. The radial basis function (RBF) kernel was used to classify soil salinization information in the study area.

### 2.5.3. Classification and Regression Tree (CART)

The classification and regression tree (CART) algorithm, introduced by Breiman [53] is a decision tree construction method [54]. CART utilizes the GINI index for node splitting, which allows it to better handle the diversity of soil spectral characteristics and the “same spectrum, different objects” phenomenon, thereby improving classification performance [55]. CART automatically selects classification features for different land cover types, establishes rules, and progressively separates the target objects, minimizing interference from other land cover types.

### 2.5.4. Classification Accuracy Assessment

Classification accuracy was evaluated using overall accuracy (OA), producer’s accuracy (PA), user’s accuracy (UA), and the Kappa coefficient. Overall accuracy refers to the ratio of correctly classified image elements to the total number of image elements. The Kappa coefficient measures the effectiveness of classification by comparing the model’s predictions with actual classification results. Producer’s and user’s accuracy were used to assess omission and commission errors for various land types [56,57].

## 2.6. Land-Use Transfer Matrix

A land-use transfer matrix [58] was employed in this study to quantitatively analyze the conversion between different land-use types, revealing their transition rates over the study period. The calculation formula for the transfer matrix is as follows:

$$S_{xy} = \begin{bmatrix} s_{11}, s_{12}, \dots, s_{1n} \\ s_{21}, s_{22}, \dots, s_{2n} \\ \vdots \\ s_{n1}, s_{n2}, \dots, s_{nn} \end{bmatrix} \quad (1)$$

where  $n$  represents land-use types, and  $S_{xy}$  denotes the area of land that transitioned from land-use type  $x$  at the beginning of the study period to saline soil type  $y$  at the end of the study period.

## 2.7. Geographical Detector

In this study, a geographical detector (Geo Detector) was used to analyze the driving factors and spatial autocorrelation of soil salinization. Geo Detector is a quantitative method



that detects the relationships between spatial variables to reveal the influence of different factors on geographic phenomena. A grid of 240 m × 240 m was created in the study area, and each unit was sampled. This method includes factor detection and interaction detection. The former assesses the contribution of individual natural factors to the spatiotemporal changes of salinization, while the latter analyzes the interactions between different factors. For detailed working principles and algorithms of Geo Detector, refer to the literature [31].

### 3. Result

#### 3.1. Mapping of Soil Salinization

##### 3.1.1. Classification Accuracy Evaluation

We calculated the overall accuracy, Kappa coefficient, user accuracy (UA), and producer accuracy (PA) using the confusion matrix to quantitatively compare the classification accuracies of the SVM and CART models, as shown in Figure 3. From 2001 to 2021, the overall classification accuracy of the CART decision tree for soil salinization was 92.78%, 85.08%, 92.64%, 91.57%, and 89.71%, with an average classification accuracy over five years of 90.36%. The corresponding Kappa coefficients were 0.9224, 0.8184, 0.8937, 0.8908, and 0.8674 over these years. For SVM, the overall classification accuracy was 79.91%, 82.83%, 86.59%, 88.84%, and 87.12%, with an average classification accuracy of 85.06%. The corresponding Kappa coefficients for the SVM model were 0.7371, 0.79, 0.8334, 0.8544, and 0.8352. As shown in Table 4, from 2001 to 2021, the user’s accuracy and producer’s accuracy of the CART method consistently outperformed the SVM model, with the average classification accuracy of CART being 5.3% higher than that of SVM.

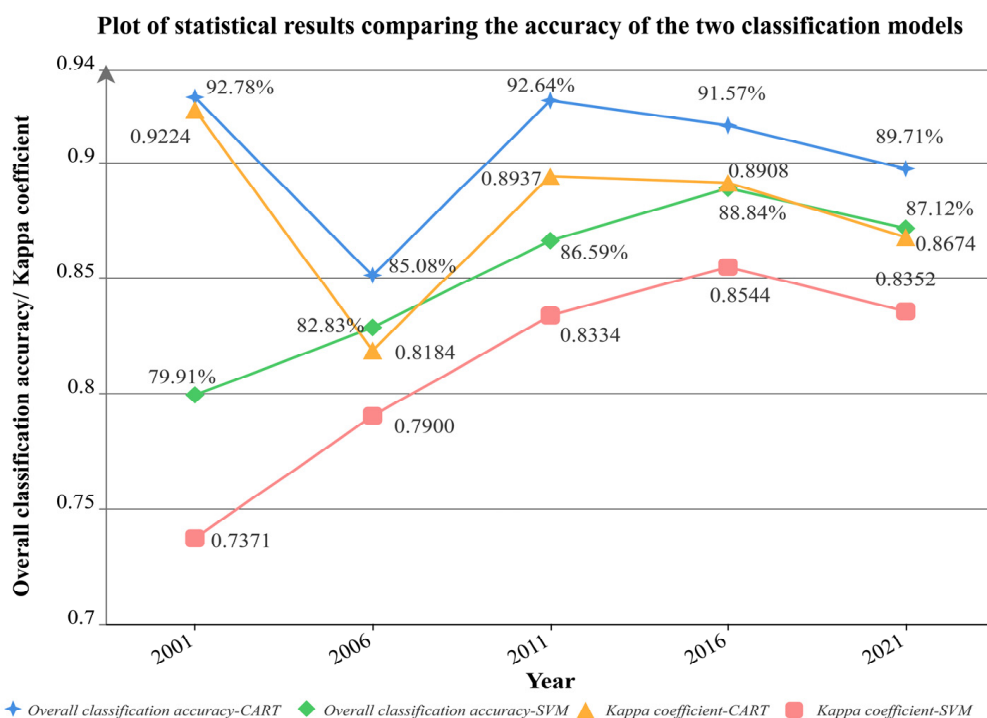


Figure 3. Sample separability and overall classification accuracy.

Table 4. Comparison of user accuracy and producer accuracy for CART and RF classifications, 2001–2021.

Method	YEAR	CLASS	PA	UA	Method	YEAR	CLASS	PA	US
CART	2001	BB	94.33	97.4	SVM	2001	BB	80.39	94.31
		WB	96.66	95.24			WB	91.62	90.53
		VG	98.47	99.78			VG	80.01	61.43

Table 4. Cont.

Method	YEAR	CLASS	PA	UA	Method	YEAR	CLASS	PA	US
		SS	66.6	72.08			SS	37.31	72.12
		MS	94.6	93.25			MS	65.03	56.5
		HS	94.69	71.7			HS	85.42	66.24
CART	2006	BB	99.17	73.65	SVM	2006	BB	91.89	63.55
		WB	89.4	99.6			WB	96.83	94.77
		VG	98.45	99.27			VG	96.97	98.67
		SS	71.31	67.95			SS	61.18	91.36
		MS	75.95	71.85			MS	88.19	72.01
		HS	57.94	98.07			HS	35.61	93.18
CART	2011	BB	93.58	93.95	SVM	2011	BB	95.8	96.9
		WB	79.81	96			WB	76.52	94.31
		VG	96.73	99.77			VG	91.27	86.1
		SS	90.11	48.78			SS	96.15	66.52
		MS	99.26	70.98			MS	51.87	92.19
		HS	93.57	80.86			HS	98.6	74.78
CART	2016	BB	95.64	94.14	SVM	2016	BB	96	99.08
		WB	89.89	84.31			WB	88.59	92.51
		VG	81.89	84.31			VG	89.95	97.47
		SS	45.22	35.45			SS	44.52	50
		MS	90.57	89.22			MS	86.87	89.12
		HS	89.29	98.12			HS	99.16	78.28
CART	2021	BB	88.91	83.35	SVM	2021	BB	94.99	89.82
		WB	93.84	90.63			WB	83.09	92.79
		VG	91.64	98.27			VG	99.1	95.55
		SS	71.53	77.69			SS	53.59	43.53
		MS	83.42	92.31			MS	84.08	84.16
		HS	79.6	68.23			HS	88.51	91.44

PA: producer's accuracy; UA: user's accuracy. SS: slightly salinized soil; MS: moderately salinized soil; HS: highly salinized soil; VG: vegetation; WB: water body; BB: bare land, desert, and building.

### 3.1.2. Classification Comparison

To compare the performance of different classification models in soil salinization mapping in detail, the year 2021 was used as a case study, concerning field sampling and observation results. The soil salinization maps generated by the SVM and CART models were compared based on classification details. Figure 4 presents the classification details of typical salinized areas within the study region. The same training samples were used to train both the SVM and CART models, but the resulting soil salinization maps showed significant differences. In this study, representative areas A and B in the Yutian Oasis were selected for local comparison. These areas are transition zones between salinized soils and deserts, characterized by high soil salinity and clearly delineated zones of mild, moderate, and severe salinization, making them ideal for validating classification performance.

The results of Figure 4 show that the SVM model performed poorly in distinguishing between severely salinized land and bare soil. In case A, an irrigation channel (BB) was misclassified as a severely salinized area (HS). In case B, the SVM model performed poorly in classifying vegetation and mildly salinized areas, with desert regions misclassified as severely and moderately salinized. This ultimately led to lower classification accuracy and performance compared to the CART model. The results indicate that the CART model, by effectively utilizing specific spectral feature sets, outperformed the SVM model in classification accuracy, particularly when dealing with complex, interwoven salinized soil regions. In contrast, the SVM model was constrained by the unfiltered original spectral feature set, potentially affected by image noise. Additionally, due to the complexity of overall soil spectral response patterns and the "same spectrum different objects" phenomenon [59], SVM did not perform as well as CART in high-precision classification. Therefore, feature

selection plays a critical role in soil salinization classification, and the CART model more effectively utilized these features, leading to superior classification performance.

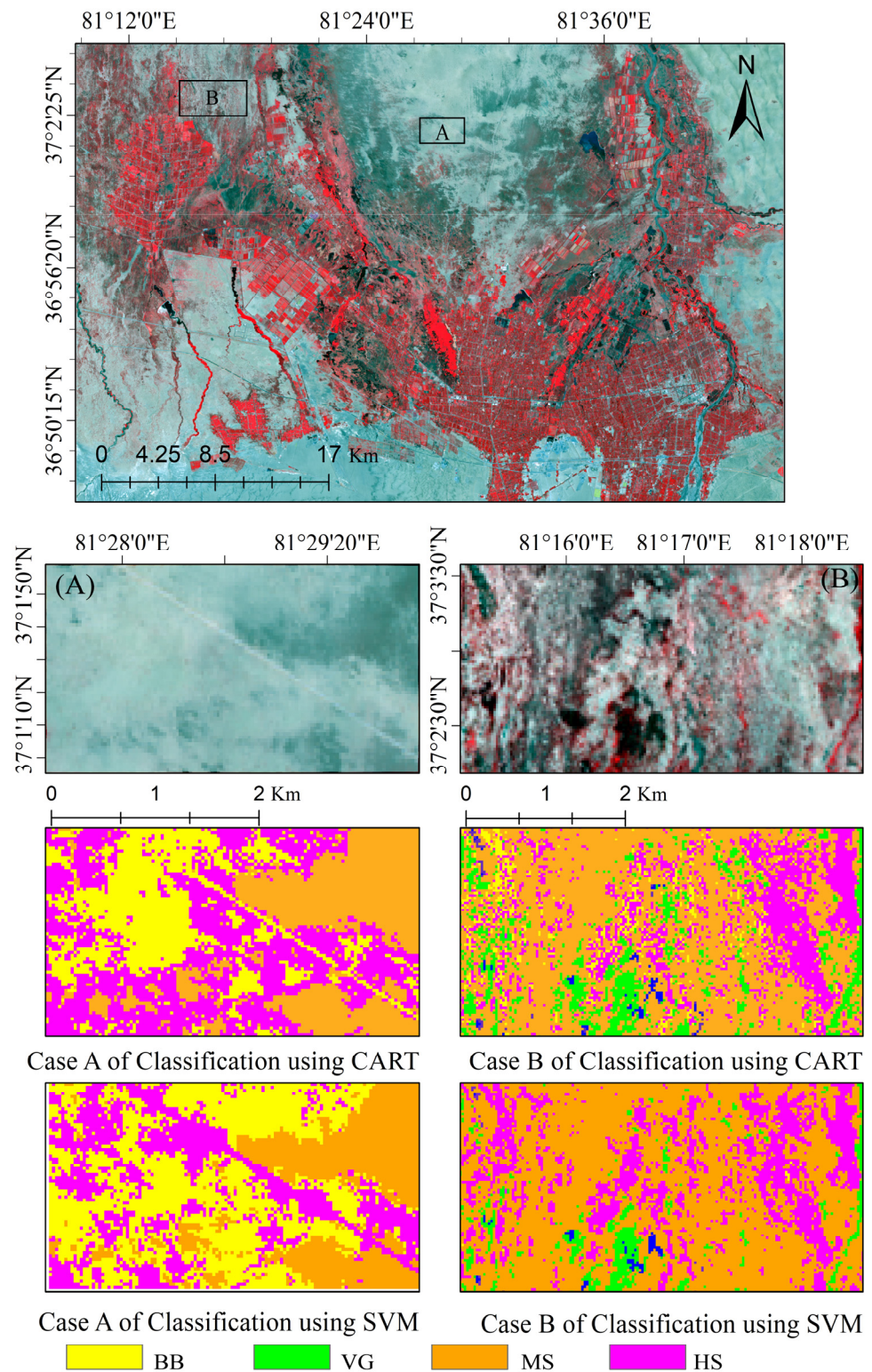


**Figure 4.** 2021 Comparison of soil salinity classification details. BB: bare land desert and building; VG: vegetation; MS: moderately salinization soil; HS: highly salinization soil; (A) Landsat8 image for case A; (B) Landsat8 image for case B.



### 3.2. Spatiotemporal Distribution Characteristics of Soil Salinization

The study utilized the CART model, which exhibited the highest classification accuracy, to generate soil salinity distribution maps from 2001 to 2021 (Figure 5). The results show that soil salinization in the Yutian Oasis primarily occurred in the northern, southwestern, and transitional zones between the oasis and desert, which is consistent with findings from previous studies [60]. This phenomenon is primarily caused by the combined effects of the local arid climate, topography, and water resource scarcity [61]. In salinized areas, severely salinized soils were primarily located near the desert boundary in the northern part of the study area and around rivers in the southwestern region, gradually transitioning into desert and barren land. In the northern desert region of the oasis, the high permeability of sandy soil and low groundwater levels result in the accumulation of salt on the soil surface as water evaporates, leading to salinization [62]. Additionally, saline lakes outside the oasis plains and salinized soils near the southwestern river are highly affected by climatic disturbances. Severely and moderately salinized soils are distributed in a banded, interwoven pattern in these areas, where high groundwater levels and intense surface evaporation significantly affect salt movement, leading to marked salt accumulation in the soil [63].

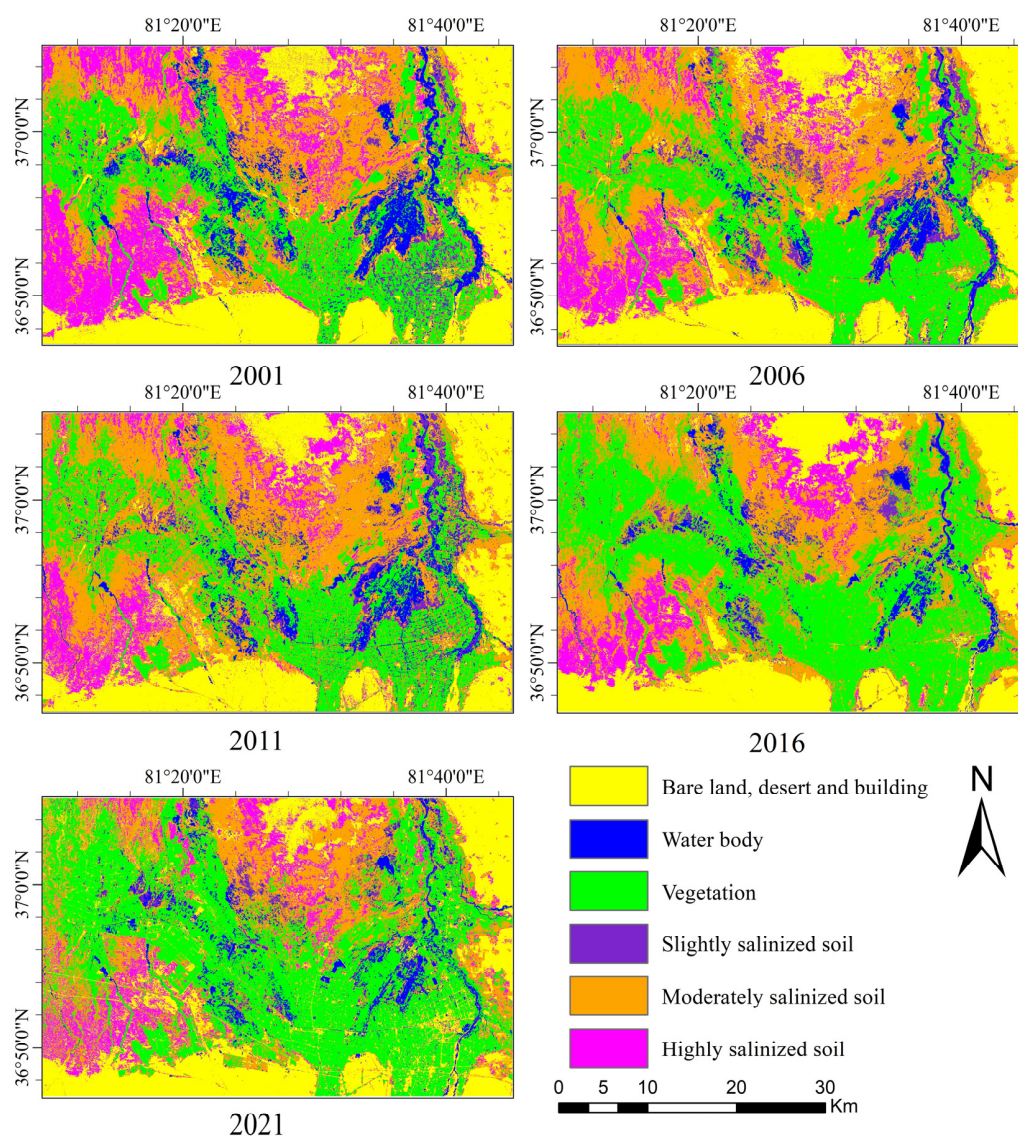


**Figure 5.** Spatiotemporal distribution of soil salinization from 2001 to 2021.



### 3.3. Spatiotemporal Transfer Analysis of Soil Salinization

To visually reflect the trend of soil salinization at different intensities, spatial overlay analysis and the difference method were employed to examine the spatiotemporal evolution of soil salinization across five periods: 2001–2006, 2006–2011, 2011–2016, 2016–2021, and 2001–2021. Different salinity weight values were assigned to each land type for each year. By calculating the difference between the new and previous time nodes, changes in soil salinization during different periods were analyzed. The calculation methods and salinity weight assignments are shown in Figure 6.

Land-use type	Weighting of salinization levels
Water body, Bare land building and desert, Vegetation	0
Slightly salinized soil	1
Moderately salinized soil	2
Highly salinized soil	3

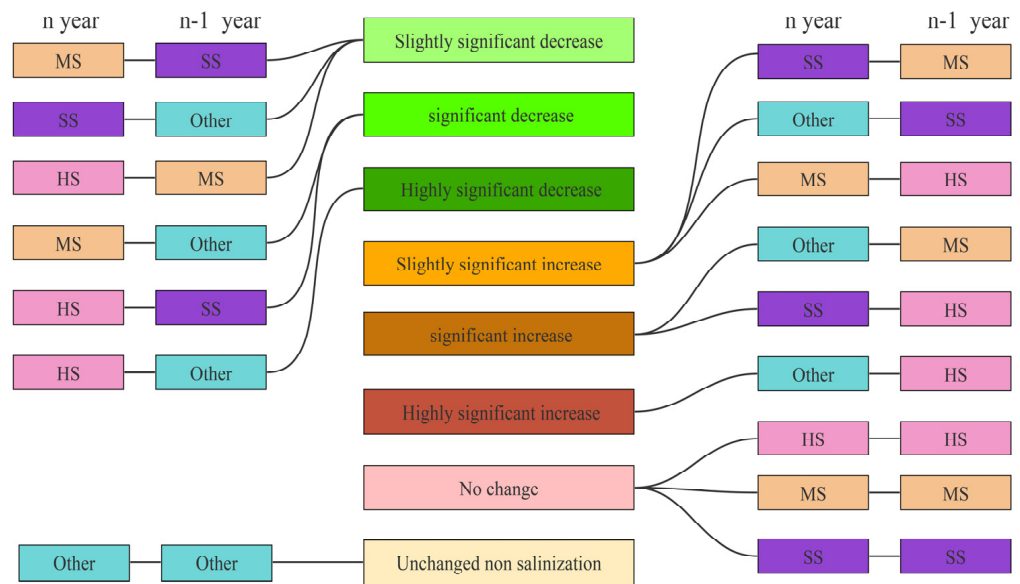


**Figure 6.** The weighting of different land types and calculation methods for spatiotemporal evolution of soil salinization. SS indicates slightly salinized soil, MS indicates moderately salinized soil, HS indicates highly salinized soil, Other indicates BB, VG, WB, BB indicates bare land building and desert, VG indicates vegetation, WB indicates water body.

Figure 7 illustrates the spatiotemporal changes in land types across the five periods from 2001 to 2021, while Figure 8 presents the land-use transitions for different types in 2001, 2006, 2011, 2016, and 2021. From the analysis of Figures 7 and 8, it is evident that from 2001 to 2021, most areas exhibited trends of slightly significant decrease, significant decrease, and highly significant decrease in salinization. This phenomenon is primarily reflected in the significant expansion of cultivated land within the oasis. According to Figure 8, vegetation cover increased significantly from 404.07 km<sup>2</sup> in 2001 to 672.89 km<sup>2</sup> in 2021, indicating a significant increase in cropland. This increase was particularly notable in the development of cultivated land in the southern Gobi desert and the eastern part of the oasis from 2011 to 2021.

The changes in water body area were not significant, with the maximum area in 2001 being 126.35 km<sup>2</sup>, which fluctuated and decreased to 98.21 km<sup>2</sup> by 2021. Nevertheless, soil moisture remains the primary driver of salt movement and changes, indirectly influencing the spatial distribution of soil salinity [64].

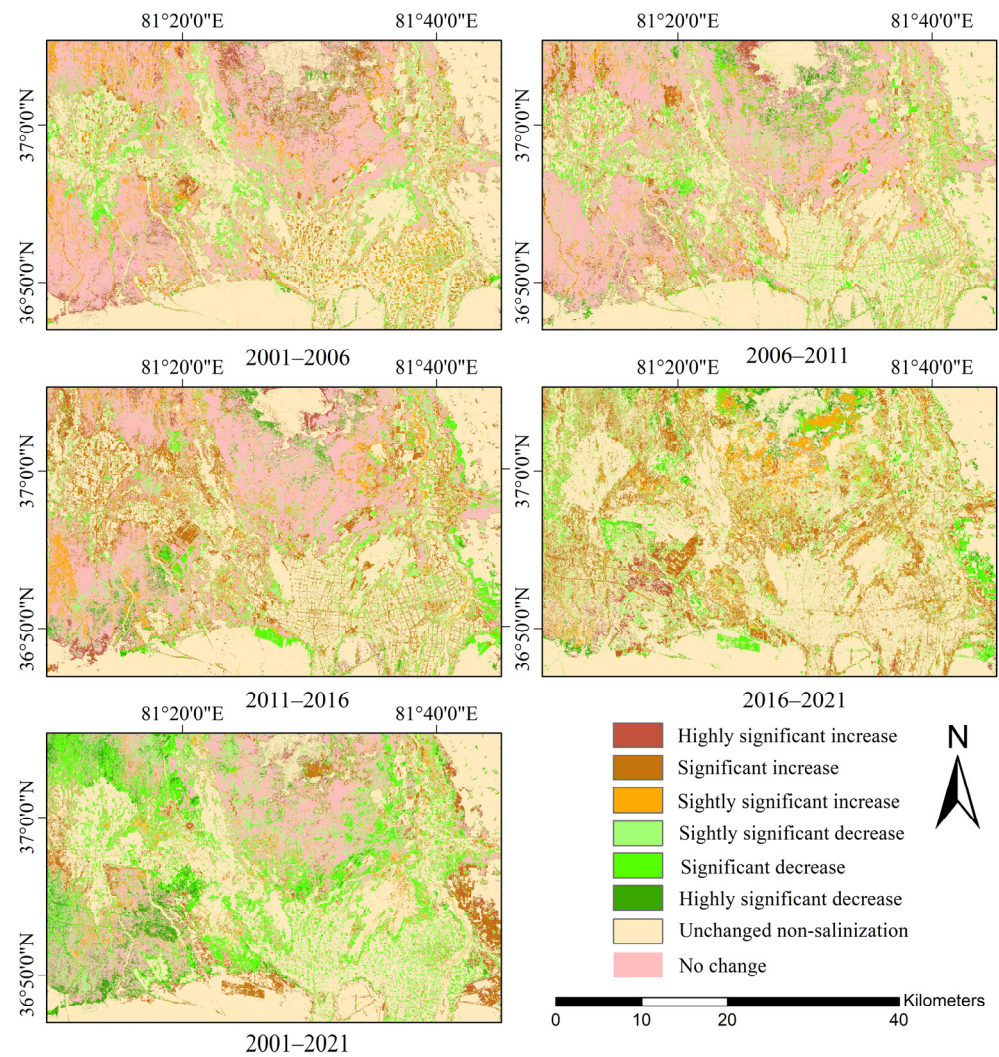


Figure 7. Spatial-temporal evolution of soil salinization in 2001–2021.

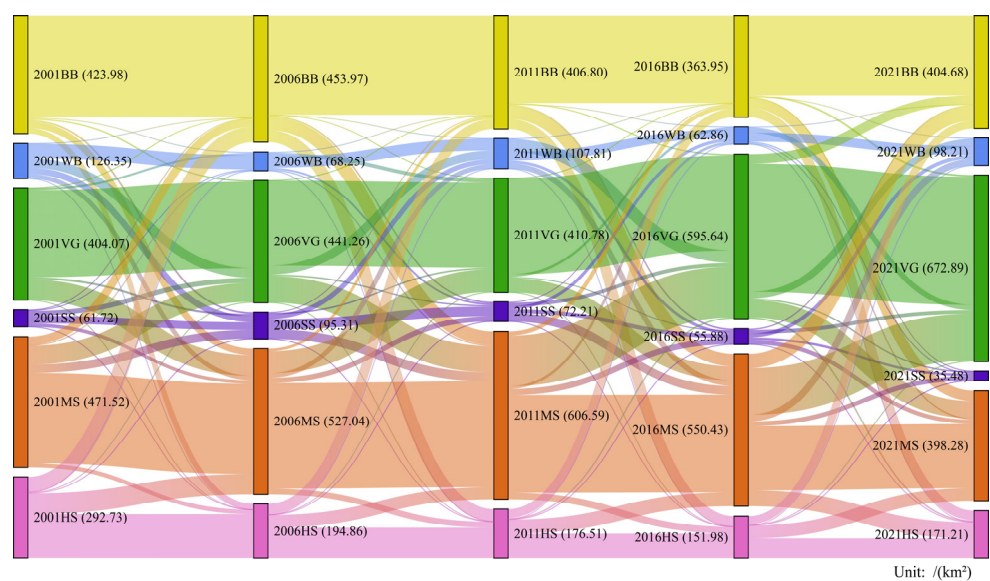


Figure 8. 2001–2021 Land transfer Sankey diagram. SS indicates slightly salinized soil, MS indicates moderately salinized soil, HS indicates highly salinized soil, BB indicates bare land, desert, and building, VG indicates vegetation, and WB indicates water body.

From 2001 to 2021, the area affected by soil salinization in the study region significantly improved, decreasing from 825.97 km<sup>2</sup> to 604.97 km<sup>2</sup>, representing a reduction of 26.76%. The area of mildly salinized soils decreased from 61.72 km<sup>2</sup> in 2001 to 35.48 km<sup>2</sup> in 2021, while moderately salinized soils initially increased and then decreased, from 471.52 km<sup>2</sup> in 2001 to 398.28 km<sup>2</sup> in 2021. Similarly, severely salinized soils showed a trend of significant increase followed by a decrease, with the area shrinking from 292.73 km<sup>2</sup> in 2001 to 171.21 km<sup>2</sup> in 2021. Noteworthy, from 2001 to 2011, the secondary salinization of cultivated land in the oasis intensified. This was mainly due to the relatively low efficiency of irrigation water use and outdated irrigation techniques, particularly the extensive use of flood irrigation, which raised the groundwater table and caused the accumulation of salts in the surface soil, leading to the conversion of mild and moderate salinized soils to severely salinized soils [65]. However, from 2011 to 2021, the area affected by various types of salinization significantly decreased, indicating that secondary salinization of cultivated land was effectively controlled. The primary reason for this improvement is the increased water use efficiency in the surface soil of cultivated land in recent years, which has reduced the trend of mildly and moderately salinized soils transforming into severely salinized areas. This achievement can be attributed to the local government's promotion of rational irrigation methods and advanced irrigation technologies, which have improved production efficiency and mitigated the trend of soil salinization [66]. In addition, key interventions such as regional water resource protection, soil conservation policies in arid regions of Northwest China [67], and the 'Three-North Shelterbelt Project' [68] were instrumental in enhancing water use efficiency, reducing desertification, and stabilizing soils, all contributing to reduced salinization [69]. These combined efforts demonstrate the effectiveness of policy interventions and technological advancements in improving soil health sustainably [70]. The observed trend in our study aligns with conclusions from previous research [63].

From 2001 to 2021, areas with little to no change in soil salinization were primarily concentrated in the transitional zones between the northern desert and salinized soils, as well as in river basins in the southwestern part of the oasis. One reason is that the northern desert has low elevation and flat terrain, leading to shallow groundwater levels, low hydraulic gradients, and stagnant horizontal runoff, creating an environment conducive to salt accumulation [71]. Another possible reason is the low irrigation water use efficiency in the cultivated land of the oasis, combined with severe field infiltration, which raises the groundwater level in the northern areas. Coupled with prolonged and intense surface evaporation during the dry season, this has resulted in the accumulation of severely and moderately salinized soils in the northern part of the oasis [33]. In the southeastern part of the oasis, the main cause of salinization could be the low salt content in cultivated land due to drainage improvement measures. However, when irrigation and drainage become imbalanced, soluble salt ions from the subsoil are transported to the surface through capillary action, leading to the formation of secondary salinization in the farmland [61].

### 3.4. The Dominant Factors in the Process of Salinization Evolution

#### 3.4.1. Single Factors

In this study, the factor detector was used to analyze and reveal the explanatory power of individual factors on the spatiotemporal evolution of salinization in the study area. By calculating the q-values of individual factors across different historical periods, the key factors influencing the evolution of soil salinization in the Yutian Oasis were identified for each period. Diagonal elements ( $X_1X_1, \dots, X_{10}X_{10}$ ) represent the results of the factor detector, reflecting the significance (q-value) of each individual factor in relation to soil salinization (classification). The higher the q-value, the greater the explanatory power of that factor in terms of the spatial heterogeneity of soil salinization, indicating a stronger correlation. The most important three factors explaining the soil salinization evolution process from 2001 to 2021 are shown in Figure 9.



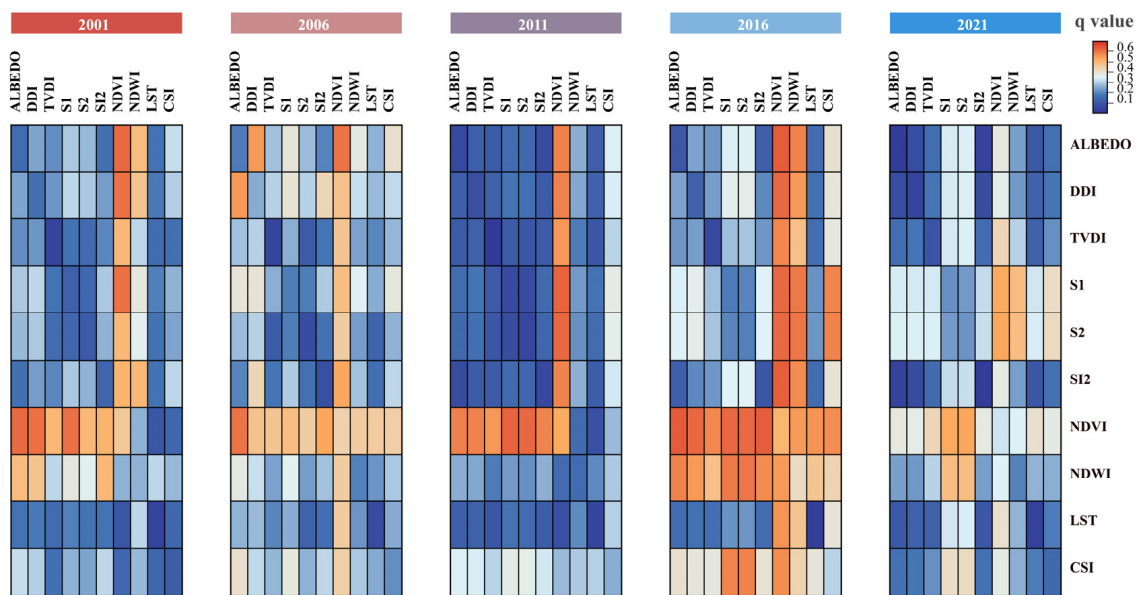


**Figure 9.** Factor detection and interaction detection results; DDI indicates desertification difference index; TVDI indicates temperature vegetation drought index; S1, S2, SI2 indicates salinity index; NDVI indicates normalized difference salinity index, NDWI indicates normalized difference water index, LST indicates land surface temperature, CSI indicates comprehensive salinity index.

For 2001: NDVI (0.46) > NDWI (0.26) > DDI (0.16); for 2006: NDVI (0.43) > DDI (0.25) > CSI (0.21); for 2011: NDVI (0.53) > CSI (0.25) > NDWI (0.14); for 2016: NDVI (0.50) > NDWI (0.41) > CSI (0.30); and for 2021: NDVI (0.33) > S2 (0.22) > S1 (0.21). These results indicate that vegetation cover is the dominant factor influencing the evolution of salinization. This is because the growth of vegetation interacts with the salt migration process in the soil [72]. Vegetation growth affects the vertical distribution of soil salts [72] which indirectly reflects the spatiotemporal distribution pattern of salt. Additionally, both NDWI and DDI represent soil moisture and water distribution in the study area, making them secondary factors influencing the evolution of salinization. The salinity index is the third most influential factor in the spatiotemporal distribution of salinization, indicating that it can, to some extent, reflect the spatiotemporal evolution of soil salinization.

### 3.4.2. Dominant Interactive Factor

The factors influencing the evolution of soil salinization in the oasis are often not singular, and the spatiotemporal evolution of soil salinization is shaped by multiple factors. In this study, an interaction detector was employed to analyze the contribution of multiple factors to the salinization process. The off-diagonal elements in reflect the explanatory power (correlation) of the interaction between any two factors ( $X_i X_j, i, j, \dots, 10$ ) on the dependent variable. The results indicate that the q-values of any two interacting factors are greater than those of individual factors, suggesting that the influence of natural factors on the salinization process is complex and mutually reinforcing. In 2001, the top three most explanatory interaction factors for the evolution of salinization in the Yutian Oasis were:  $NDVI \cap Albedo$  (0.52) >  $NDVI \cap DDI$  (0.51) >  $NDVI \cap S1$  (0.51). In 2006, they were:  $NDVI \cap Albedo$  (0.61) >  $Albedo \cap DDI$  (0.55) >  $NDVI \cap SI2$  (0.54).  $NDVI \cap Albedo$  (0.61) >  $Albedo \cap DDI$  (0.55) >  $NDVI \cap SI2$  (0.54). For 2011:  $NDVI \cap S1$  (0.63) >  $NDVI \cap S2$  (0.62) >  $NDVI \cap Albedo$  (0.59). For 2016:  $NDWI \cap S2$  (0.60) >  $NDWI \cap S1$  (0.59) >  $CSI \cap S2$  (0.58). And for 2021:  $NDVI \cap S2$  (0.53) >  $NDVI \cap S1$  (0.53) >  $NDWI \cap S2$  (0.49). In conclusion, NDVI and NDWI were the primary interactive factors influencing the spatiotemporal evolution of salinization in the study area, indicating that vegetation and soil moisture jointly affect the migration and accumulation of salts within the soil, thereby controlling the spatial heterogeneity of salinization. Vegetation not only impacts evap-



otranspiration rates but also modulates the soil moisture regime, which in turn affects salt mobilization. This interdependence underscores the importance of considering both vegetation dynamics and soil moisture availability when evaluating salinization processes.

#### 4. Discussion

The Yutian Oasis, significantly affected by seasonal climatic variations, represents a typical arid region exhibiting both secondary and primary salinization phenomena. Previous studies have mostly focused on discussing the spatiotemporal variation trends of oasis soil salinization using medium-resolution satellite imagery and assessing mapping accuracy via confusion matrices, without further exploration into the evolution and driving factors of soil salinization. This study integrated Landsat imagery with machine learning methods to map and monitor soil salinization dynamically under medium-scale conditions. The classification results were discussed based on field sampling and surveys, providing valuable insights for regional-scale soil salinization monitoring.

##### 4.1. Dominant Factors in the Spatiotemporal Evolution of Modern Yutian Oasis Soil Salinization

The spatial distribution of salt content in the soil profiles of the Yutian Oasis results from the combined action of various factors, including structural factors (such as climate, parent material, topography, soil types, and groundwater movement) and random factors (such as farming practices, fertilization, cropping systems, and irrigation schemes) [60]. In this study, most natural factors had  $q$ -values less than 0.6, indicating their limited explanatory power for the spatial heterogeneity of salinization. This indicates that the correlation between individual factors and the spatial distribution of salinization is not significant, while also revealing notable spatial clustering (spatial autocorrelation) of salinization in the study area. This spatial autocorrelation can be attributed to the clustering of salinization in specific areas. Extensive spatial clustering of salinization was observed in the northern and western parts of the study area, resulting in relatively uniform distribution patterns and weak spatial heterogeneity, consistent with the findings of previous studies [60]. Thus, the  $q$ -values of any two interacting factors were higher than those of individual factors, indicating that multi-factor interactions determine the spatial heterogeneity of soil salinization.

Based on our field surveys conducted from 2021 to 2024, the promotion of modern irrigation technologies such as drip irrigation, Unmanned Aerial Vehicle (UAV) spraying, and subsurface drainage systems [73] has significantly improved water use efficiency in oasis farmland [74,75], reducing salt accumulation in cultivated land and leading to a marked improvement in secondary salinization in the region.

Additionally, future research should explore the specific effects of groundwater depth and soil profiles on salinization accumulation [76–78], further quantifying the role of natural and social factors in the dynamic changes of oasis salinization.

##### 4.2. Limitations and Prospects

The comparison between SVM and CART models highlights the strengths of CART in classifying soil salinization with higher overall accuracy and Kappa coefficients. While CART is known for its simplicity and interpretability due to its decision tree structure, it excels in handling complex data with varied spectral characteristics, making it effective for distinguishing classes in heterogeneous environments. Random forest (RF) also uses decision trees but in an ensemble format, combining multiple decision trees to enhance overall model stability and reduce overfitting [79]. This ensemble approach, however, can dilute the precise feature selection advantage that CART provides, especially in cases where distinct feature splits are critical for addressing the “same spectrum, different objects” phenomenon. Although RF is typically more robust and adept at handling larger datasets, CART may be better suited for specific, targeted classifications in complex spectral conditions [80], such as arid regions with bare soil and sparse vegetation. Nevertheless, RF has demonstrated potential in constructing effective salinization inversion models, offering

flexibility and improved accuracy through its ensemble learning framework, which could be leveraged for broader applications in soil salinity mapping [81–83].

Field investigations over the years have revealed that the distribution of saline soils in the study area is highly complex, with salinized land of varying degrees showing “fragmented” distribution within a 10-m range. This indicates that the 30-m spatial resolution of Landsat imagery hinders the accurate identification of smaller or dispersed saline soil patches, leading to mixed-pixel effects where different land features are represented within the same pixel. Previous studies have demonstrated the great potential of using high-resolution satellite imagery such as Planet Scope for soil salinization inversion [84,85]. Therefore, to overcome these limitations, employing higher spatial resolution imagery and remote sensing platforms can significantly improve the accuracy of soil salinization mapping.

To compare the mapping performance at different spatial resolutions, this study used 3m resolution Planet Scope imagery to map soil salinization in the Case A region.

As shown in Figure 10, at 30-m resolution, Landsat imagery failed to effectively distinguish between impervious surfaces (BB, building desert and bare land) and highly salinized soil (HS, highly salinization soil), and the canal in the upper-left corner was incorrectly classified. The Case A region is located in the northern part of the study area, at the intersection of desert and salinized land, where salt-tolerant vegetation such as tamarisk, salt cedar, and reeds covers an area much smaller than 30 m, resulting in spectral characteristics prone to mixed-pixel effects. The Kappa coefficient and overall accuracy for classification of planet scope images using the SVM model are 0.9101 and 94.304% respectively, while the Kappa coefficient and overall accuracy using landsat8 are 0.8352 and 87.12%. Therefore, using high-resolution imagery can not only reduce mixed pixels but also improve the classification accuracy of spectrally similar features such as highly salinized soil and impervious surfaces, thereby enhancing the overall accuracy of regional salinization monitoring.

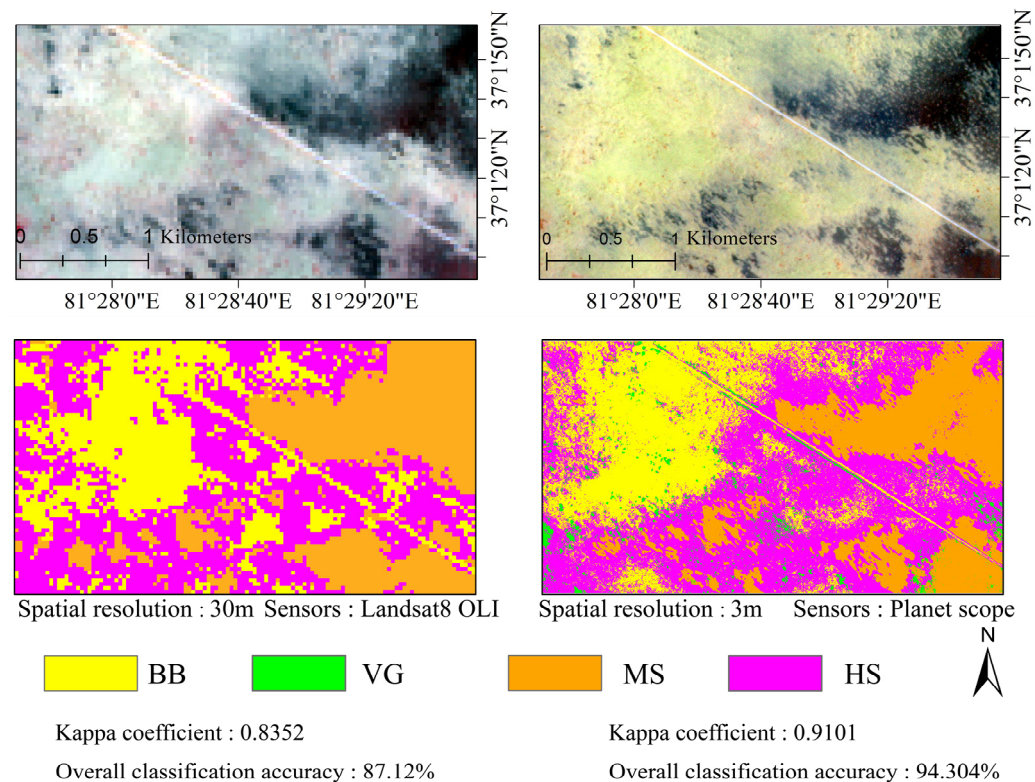


**Figure 10.** Landsat8 OLI compared to Planet scope for salinization soil classification in 2021; MS indicates moderately salinized soil, HS indicates highly salinized soil, BB indicates Bare land building and desert, VG indicates Vegetation.

Optical remote sensing (such as Landsat and Sentinel-2) excels in providing surface reflectance information, enabling the identification of vegetation cover, water bodies, and bare soil. Microwave remote sensing (such as SAR imagery), on the other hand, has the ability to penetrate the soil surface, capturing soil moisture content and salinity dynamics, making it particularly advantageous in arid regions. Combining optical and microwave imagery enables multi-dimensional monitoring of soil salinization and provides more accurate classification results. Several studies [33,63] have shown that integrating backscatter coefficients, polarization features, and phase characteristics from optical and microwave remote sensing can significantly improve the classification accuracy of salinized soils [77,86,87]. Moreover, multi-source fusion of multispectral remote sensing data (such as Sentinel-2 or other high-resolution satellite data) can provide richer soil information in salinization monitoring, further enhancing classification performance [88].

To further improve classification performance, the integration of advanced machine learning methods, such as random forest (RF), convolutional neural networks (CNN), and gradient boosting, can be particularly beneficial. These machine learning models are capable of capturing complex spatial and spectral features effectively, thereby addressing limitations such as mixed pixels and similar spectral characteristics that are common in salinized areas. Additionally, combining multi-source remote sensing data, particularly high spatial resolution imagery, with machine learning models tailored to the study area can enhance the precision of soil salinization monitoring [89].

Furthermore, the accuracy of machine learning classification methods largely depends on the quality and quantity of training samples. Therefore, to comprehensively capture the spatiotemporal trends of salinization, sample points should encompass various soil types across different geographic locations and ecological conditions within the study area. Future research should focus on enhancing the diversity and representativeness of sample data. By training models with diverse sample sets, the model's generalization ability across different regions and scenarios can be improved, minimizing classification errors and ensuring higher accuracy in dynamic salinization monitoring [7].

These studies will provide more detailed and valuable references for regional forest and grassland conservation, and ecological restoration. By integrating higher resolution remote sensing data with multi-dimensional environmental variable analysis, future research is expected to achieve a more comprehensive understanding of salinization processes and offer insights for salinization prevention in similar regions worldwide.

## 5. Conclusions

Soil salinization has had a significant impact on agricultural production and ecological environments globally, making effective and rapid monitoring of soil salinization essential. This study aims to achieve dynamic monitoring of soil salinization using remote sensing and spatial information technology. By comparing the SVM and CART models, we confirmed the superiority of CART in extracting salinization information and further employed the CART model to map the spatiotemporal distribution of soil salinization in the Yutian Oasis, revealing its evolution and driving factors.

The results indicate that:

- (1) The classification accuracy of the CART model was significantly higher than that of the SVM model, with an average improvement of 5.3%. The CART model exhibited superior detail-capturing ability in complex salinized regions, particularly in distinguishing between highly salinized soil and bare land. It was able to utilize spectral features to better reflect the actual salinization conditions, whereas the SVM model performed poorly in these areas. This finding supports the applicability of using the CART model for spatiotemporal dynamic monitoring of soil salinization.
- (2) From 2001 to 2021, the area affected by soil salinization decreased by 26.76%, from 825.97 km<sup>2</sup> to 604.97 km<sup>2</sup>, with significant improvements, particularly in heavily salinized areas. The alleviation of secondary salinization was mainly concentrated in the cultivated lands within the oasis, while the expansion of cultivated land at the oasis

periphery also significantly reduced the spread of salinization. This improvement was attributed to the promotion of modern agricultural irrigation technologies and the enhancement of land use efficiency.

- (3) The results of the Geo Detector analysis indicated that NDVI (Normalized Difference Vegetation Index) was the primary factor influencing soil salinization dynamics, with the highest q-value reaching 0.53. Additionally, factors such as NDWI (Normalized Difference Water Index) and CSI (Comprehensive Salinity Index) also significantly impacted the spatial distribution of salinization. Interaction analysis showed that the interaction between NDVI and NDWI explained the major drivers of spatiotemporal changes in salinization, indicating that vegetation cover and soil moisture jointly determine the dynamic evolution of soil salinization.

This study comprehensively analyzed the distribution, trends, and driving factors of soil salinization in the Yutian Oasis, providing a scientific basis for the sustainable use of regional land resources. The results offer valuable insights for local governments in formulating irrigation strategies and land use management, contributing to the mitigation of land degradation and the improvement of the ecological environment.

**Author Contributions:** S.L. and I.N. designed the study. S.L., J.S., X.L., X.Y. and Y.A. collected data. S.L. formed the data analysis and drafted the manuscript. I.N. coordinated and supervised the study, and I.N. managed and coordinated responsibility for the research activity planning and execution. All authors have read and agreed to the published version of the manuscript.

**Funding:** This research was funded by The National Natural Science Foundation of China, (No. 42061065, No. 32160319), The Natural Science Foundation of Xinjiang Uygur Autonomous Region, China (No. 2024D01C34), and The Third Xinjiang Comprehensive Scientific Expedition (No. 2022xjkk0300).

**Data Availability Statement:** Data will be made available on request; further inquiries can be directed to the corresponding author.

**Acknowledgments:** All authors are sincerely grateful to the reviewers and editors for their constructive comments on the improvement of the manuscript.

**Conflicts of Interest:** The authors declare that there are no conflicts of interest or competing financial interests in relation to the work described in this manuscript. All authors have reviewed and approved the final version of the manuscript and agree to its submission. The research was conducted in the absence of any commercial or financial relationships that could be construed as a potential conflict of interest.

## References

1. Wang, Y.; Deng, C.; Liu, Y.; Niu, Z.; Li, Y. Identifying change in spatial accumulation of soil salinity in an inland river watershed, China. *Sci. Total Environ.* **2018**, *621*, 177–185. [[CrossRef](#)] [[PubMed](#)]
2. Peng, J.; Biswas, A.; Jiang, Q.; Zhao, R.; Hu, J.; Hu, B.; Shi, Z. Estimating soil salinity from remote sensing and terrain data in southern Xinjiang Province, China. *Geoderma* **2019**, *337*, 1309–1319. [[CrossRef](#)]
3. Song, C.; Ren, H.; Huang, C. Estimating Soil Salinity in the Yellow River Delta, Eastern China—An Integrated Approach Using Spectral and Terrain Indices with the Generalized Additive Model. *Pedosphere* **2016**, *26*, 626–635. [[CrossRef](#)]
4. Chen, H.Y.; Zhao, G.X.; Li, Y.H.; Wang, D.Y.; Ma, Y. Monitoring the seasonal dynamics of soil salinization in the Yellow River delta of China using Landsat data. *Nat. Hazards Earth Syst. Sci.* **2019**, *19*, 1499–1508. [[CrossRef](#)]
5. Abbas, A.; Khan, S.; Hussain, N.; Hanjra, M.A.; Akbar, S. Characterizing soil salinity in irrigated agriculture using a remote sensing approach. *Phys. Chem. Earth* **2013**, *55–57*, 43–52. [[CrossRef](#)]
6. Ahmed, Z.; Iqbal, J. Evaluation of Landsat TM5 Multispectral Data for Automated Mapping of Surface Soil Texture and Organic Matter in GIS. *Eur. J. Remote Sens.* **2014**, *47*, 557–573. [[CrossRef](#)]
7. Sahbeni, G.; Ngabire, M.; Musyimi, P.K.; Székely, B. Challenges and Opportunities in Remote Sensing for Soil Salinization Mapping and Monitoring: A Review. *Remote Sens.* **2023**, *15*, 2540. [[CrossRef](#)]
8. Yu, X.Y.; Xin, P.; Hong, L. Effect of evaporation on soil salinization caused by ocean surge inundation. *J. Hydrol.* **2021**, *597*, 126200. [[CrossRef](#)]
9. Xie, X.F.; Pu, L.J.; Zhu, M.; Xu, Y.; Wang, X.H. Linkage between soil salinization indicators and physicochemical properties in a long-term intensive agricultural coastal reclamation area, Eastern China. *J. Soils Sediments* **2019**, *19*, 3699–3707. [[CrossRef](#)]



10. Dong, F.; Tang, Y.J.; Xing, X.R.; Liu, Z.H.; Xing, L.T. Formation and Evolution of Soil Salinization in Shouguang City Based on PMS and OLI/TM Sensors. *Water* **2019**, *11*, 345. [[CrossRef](#)]
11. Mu, Q.; Shengbin, Z.; Lei, L.U.; Junjie, Y.A.N.; Heping, L.I. Temporal and spatial changes of soil salinization and improved countermeasures of Tarim Basin Irrigation District in recent 25 a. *Arid Land Geogr.* **2011**, *34*, 604–613.
12. Zhang, Z.M.; Fan, Y.G.; Zhang, A.Z.; Jiao, Z.J. Baseline-Based Soil Salinity Index (BSSI): A Novel Remote Sensing Monitoring Method of Soil Salinization. *IEEE J. Sel. Top. Appl. Earth Obs. Remote Sens.* **2023**, *16*, 202–214. [[CrossRef](#)]
13. Ma, Y.X.; Tashpolat, N. Remote Sensing Monitoring of Soil Salinity in Weigan River-Kuqa River Delta Oasis Based on Two-Dimensional Feature Space. *Water* **2023**, *15*, 1694. [[CrossRef](#)]
14. Padarian, J.; Minasny, B.; McBratney, A.B. Machine learning and soil sciences: A review aided by machine learning tools. *Soil* **2020**, *6*, 35–52. [[CrossRef](#)]
15. Wadoux, A.M.J.C.; Minasny, B.; McBratney, A.B. Machine learning for digital soil mapping: Applications, challenges and suggested solutions. *Earth-Sci. Rev.* **2020**, *210*, 103359. [[CrossRef](#)]
16. Vermeulen, D.; Van Niekerk, A. Machine learning performance for predicting soil salinity using different combinations of geomorphometric covariates. *Geoderma* **2017**, *299*, 1–12. [[CrossRef](#)]
17. Wang, F.; Yang, S.; Yang, W.; Yang, X.; Ding, J. Comparison of machine learning algorithms for soil salinity predictions in three dryland oases located in Xinjiang Uyghur Autonomous Region (XJUAR) of China. *Eur. J. Remote Sens.* **2019**, *52*, 256–276. [[CrossRef](#)]
18. Li, H.; Liu, X.; Hu, B.; Biswas, A.; Jiang, Q.; Liu, W.; Wang, N.; Peng, J. Field-Scale Characterization of Spatio-Temporal Variability of Soil Salinity in Three Dimensions. *Remote Sens.* **2020**, *12*, 4043. [[CrossRef](#)]
19. Salem, O.H.; Jia, Z. Evaluation of Different Soil Salinity Indices Using Remote Sensing Techniques in Siwa Oasis, Egypt. *Agronomy* **2024**, *14*, 723. [[CrossRef](#)]
20. Ding, J.; Zhang, Z.; Li, X.; Yan, X. Assessment of dynamic evolution on soil salinization of an oasis in Turkmenistan of Central Asia. *Arid Land Geogr.* **2013**, *36*, 571–578.
21. Rukhovich, D.I.; Pankova, E.I.; Chernousenko, G.I.; Koroleva, P.V. Long-term salinization dynamics in irrigated soils of the Golodnaya Steppe and methods of their assessment on the basis of remote sensing data. *Eurasian Soil Sci.* **2010**, *43*, 682–692. [[CrossRef](#)]
22. Stasyuk, N.V. Temporal dynamics of soil cover salinization in the Terek delta. *Russ. J. Ecol.* **2001**, *32*, 22–28. [[CrossRef](#)]
23. Xiao, Y.; Zhao, G.X.; Li, T.; Zhou, X.; Li, J.M. Soil salinization of cultivated land in Shandong Province, China—Dynamics during the past 40 years. *Land Degrad. Dev.* **2019**, *30*, 426–436. [[CrossRef](#)]
24. Tran, T.V.; Tran, D.X.; Myint, S.W.; Huang, C.-y.; Pham, H.V.; Luu, T.H.; Vo, T.M.T. Examining spatiotemporal salinity dynamics in the Mekong River Delta using Landsat time series imagery and a spatial regression approach. *Sci. Total Environ.* **2019**, *687*, 1087–1097. [[CrossRef](#)] [[PubMed](#)]
25. Jabbar, M.T.; Zhou, J.X. Assessment of Soil Salinity Risk on the Agricultural Area in Basrah Province, Iraq: Using Remote Sensing and GIS Techniques. *J. Earth Sci.* **2012**, *23*, 881–891. [[CrossRef](#)]
26. Howari, F.M.; Goodell, P.C.; Miyamoto, S. Spectral properties of salt crusts formed on saline soils. *J. Environ. Qual.* **2002**, *31*, 1453–1461. [[CrossRef](#)]
27. Guo, B.; Liu, Y.F.; Fan, J.F.; Lu, M.; Zang, W.Q.; Liu, C.; Wang, B.Y.; Huang, X.Z.; Lai, J.B.; Wu, H.W. The salinization process and its response to the combined processes of climate change-human activity in the Yellow River Delta between 1984 and 2022. *Catena* **2023**, *231*, 107301. [[CrossRef](#)]
28. Song, Y.; Gao, M.; Wang, Z.; Gong, T.; Chen, W. Spatio-Temporal Variability Characteristics of Coastal Soil Salinization and Its Driving Factors Detection. *Water* **2022**, *14*, 3326. [[CrossRef](#)]
29. Bai, L.; Zhou, J.; Luo, J.; Dou, H.; Zhang, Y. Analyzing Driving Factors of Soil Alkalinization Based on Geodetector—A Case in Northeast China. *Sustainability* **2023**, *15*, 1538. [[CrossRef](#)]
30. Duan, Y.; Ma, L.; Abuduwaili, J.; Liu, W.; Saparov, G.; Smanov, Z. Driving Factor Identification for the Spatial Distribution of Soil Salinity in the Irrigation Area of the Syr Darya River, Kazakhstan. *Agronomy* **2022**, *12*, 1912. [[CrossRef](#)]
31. Wang, J.; Xu, C. Geodetector: Principle and prospective. *Acta Geogr. Sin.* **2017**, *72*, 116–134.
32. Li, X.; Li, Y.; Wang, B.; Sun, Y.; Cui, G.; Liang, Z. Analysis of spatial-temporal variation of the saline-sodic soil in the west of Jilin Province from 1989 to 2019 and influencing factors. *Catena* **2022**, *217*, 106492. [[CrossRef](#)]
33. Ilyas, N.; Shi, Q.; Abdulla, A.; Xia, N.; Wang, J. Quantitative evaluation of soil salinization risk in Keriya Oasis based on grey evaluation model. *Trans. Chin. Soc. Agric. Eng.* **2019**, *35*, 176–184.
34. Du, M.; Li, L.; Luo, G.; Dong, K.; Shi, Q. Effects of Climate and Land Use Change on Agricultural Water Consumption in Yutian Oasis. *Bull. Soil Water Conserv.* **2020**, *40*, 103–109.
35. Zaytungul, Y.; Mamat, S.; Abdusalam, A.; Zhang, D. Soil salinity inversion in Yutian Oasis based on PALSAR radar data. *Resour. Sci.* **2018**, *40*, 2110–2117.
36. Zhu, C.M.; Ding, J.L.; Zhang, Z.P.; Wang, J.J.; Chen, X.Y.; Han, L.J.; Shi, H.B.; Wang, J.Z. Soil salinity dynamics in arid oases during irrigated and non-irrigated seasons. *Land Degrad. Dev.* **2023**, *34*, 3823–3835. [[CrossRef](#)]
37. Hassani, A.; Azapagic, A.; Shokri, N. Global predictions of primary soil salinization under changing climate in the 21st century. *Nat. Commun.* **2021**, *12*, 6663. [[CrossRef](#)]

38. Douaoui, A.E.K.; Nicolas, H.; Walter, C. Detecting salinity hazards within a semiarid context by means of combining soil and remote-sensing data. *Geoderma* **2006**, *134*, 217–230. [[CrossRef](#)]
39. Abbas, A.; Khan, S. *Using Remote Sensing Techniques for Appraisal of Irrigated Soil Salinity*; Modeling and Simulation Society of Australia and New Zealand: Canberra, Australia, 2007.
40. Rouse, J.W.; Haas, R.H.; Schell, J.A.; Deering, D.W. *Monitoring Vegetation Systems in the Great Plains with ERTS*; NASA Special Publications: Washington, DC, USA, 1974.
41. Khan, N.M.; Rastoskuev, V.V.; Sato, Y.; Shiozawa, S. Assessment of hydrosaline land degradation by using a simple approach of remote sensing indicators. *Agric. Water Manag.* **2005**, *77*, 96–109. [[CrossRef](#)]
42. Bannari, A.; Guedon, A.M.; El-Harti, A.; Cherkaoui, F.Z.; El-Ghmari, A. Characterization of Slightly and Moderately Saline and Sodic Soils in Irrigated Agricultural Land using Simulated Data of Advanced Land Imaging (EO-1) Sensor. *Commun. Soil Sci. Plant Anal.* **2008**, *39*, 2795–2811. [[CrossRef](#)]
43. Allbed, A.; Kumar, L.; Aldakheel, Y.Y. Assessing soil salinity using soil salinity and vegetation indices derived from IKONOS high-spatial resolution imageries: Applications in a date palm dominated region. *Geoderma* **2014**, *230*, 1–8. [[CrossRef](#)]
44. Pettorelli, N.; Vik, J.O.; Mysterud, A.; Gaillard, J.M.; Tucker, C.J.; Stenseth, N.C. Using the satellite-derived NDVI to assess ecological responses to environmental change. *Trends Ecol. Evol.* **2005**, *20*, 503–510. [[CrossRef](#)] [[PubMed](#)]
45. Barsi, J.A.; Barker, J.L.; Schott, J.R. An atmospheric correction parameter calculator for a single thermal band earth-sensing instrument. In Proceedings of the IGARSS 2003. 2003 IEEE International Geoscience and Remote Sensing Symposium. Proceedings (IEEE Cat. No. 03CH37477), Toulouse, France, 21–25 July 2003; pp. 3014–3016.
46. Barsi, J.A.; Schott, J.R.; Palluconi, F.D.; Hook, S.J. Validation of a web-based atmospheric correction tool for single thermal band instruments. In Proceedings of the Earth Observing Systems X, San Diego, CA, USA, 31 July–4 August 2005; pp. 136–142.
47. Becker, F.; Li, Z.-L. Temperature-independent spectral indices in thermal infrared bands. *Remote Sens. Environ.* **1990**, *32*, 17–33. [[CrossRef](#)]
48. Liang, S.L. Narrowband to broadband conversions of land surface albedo I Algorithms. *Remote Sens. Environ.* **2001**, *76*, 213–238. [[CrossRef](#)]
49. Verstraete, M.M.; Pinty, B. Designing optimal spectral indexes for remote sensing applications. *IEEE Trans. Geosci. Remote Sens.* **1996**, *34*, 1254–1265. [[CrossRef](#)]
50. Sandholt, I.; Rasmussen, K.; Andersen, J. A simple interpretation of the surface temperature/vegetation index space for assessment of surface moisture status. *Remote Sens. Environ.* **2002**, *79*, 213–224. [[CrossRef](#)]
51. Scudiero, E.; Skaggs, T.H.; Corwin, D.L. Regional-scale soil salinity assessment using Landsat ETM plus canopy reflectance. *Remote Sens. Environ.* **2015**, *169*, 335–343. [[CrossRef](#)]
52. Vapnik, V.N. An overview of statistical learning theory. *IEEE Trans. Neural Netw.* **1999**, *10*, 988–999. [[CrossRef](#)]
53. Breiman, L. *Classification and Regression Trees*; Routledge: London, UK, 2017.
54. Loh, W.Y. Classification and regression trees. *Wiley Interdiscip. Rev. Data Min. Knowl. Discov.* **2011**, *1*, 14–23. [[CrossRef](#)]
55. Li, Y.; Liu, H. Advance in Wetland Classification and Wetland Landscape Classification Researches. *Wetl. Sci.* **2014**, *12*, 102–108.
56. Liu, C.; Frazier, P.; Kumar, L. Comparative assessment of the measures of thematic classification accuracy. *Remote Sens. Environ.* **2007**, *107*, 606–616. [[CrossRef](#)]
57. Deng, Y.; Jiang, W.; Wang, X.; Peng, K. Refined wetland classification of international wetland cities based on the random forest algorithm and knowledge-driven rules: A case study of Changde city, China. *Natl. Remote Sens. Bull.* **2023**, *27*, 1426–1440.
58. Jia, T.; Hu, X. Spatiotemporal Dynamic Evolution Characteristics of Land Use in China's Two Screens and Three Belts' Ecological Barrier Areas from 1985 to 2020. *Res. Soil Water Conserv.* **2024**, *31*, 348–363.
59. He-ping, L.I.; Chang-yan, T.; Mu, Q.; Shi-xin, W.U. On remote sensing data interpretation key and index of saline soil of arable land in Xinjiang. *Agric. Res. Arid Areas* **2009**, *27*, 218–222.
60. Mamat, Z.; Yimit, H.; Lv, Y. Spatial Distributing Pattern of Salinized Soils and their Salinity in Typical Area of Yutian Oasis. *J. Soil Sci.* **2013**, *44*, 1314–1320.
61. Zhao, J.; Nurmemet, I.; Muhetaer, N.; Xiao, S.; Abulaiti, A. Monitoring Soil Salinity Using Machine Learning and the Polarimetric Scattering Features of PALSAR-2 Data. *Sustainability* **2023**, *15*, 7452. [[CrossRef](#)]
62. Wu, J.H.; Li, P.Y.; Qian, H.; Fang, Y. Assessment of soil salinization based on a low-cost method and its influencing factors in a semi-arid agricultural area, northwest China. *Environ. Earth Sci.* **2014**, *71*, 3465–3475. [[CrossRef](#)]
63. Xiao, S.; Ilyas, N.; Nuerbiye, M.; Zhao, J.; Adilai, A. Spatial and temporal analysis of soil salinity in Yutian Oasis by combined optical and radar multi-source remote sensing. *Arid Zone Res.* **2023**, *40*, 59–68.
64. Yang, J.S.; Yao, R.J. Spatial Variability of Soil Water and Salt Characteristics in the Yellow River Delta. *Sci. Geogr. Sin.* **2007**, *27*, 348–353.
65. Yuan, Y.-y.; Halik, W.; Guan, J.-y.; Lu, L.-h.; Zhang, Q.-q. Spatial differentiation and impact factors of Yutian Oasis' s soil surface salt based on GWR model. *Chin. J. Appl. Ecol.* **2016**, *27*, 3273–3282. [[CrossRef](#)]
66. Zhuang, Q.W.; Shao, Z.F.; Huang, X.; Zhang, Y.; Wu, W.F.; Feng, X.X.; Lv, X.W.; Ding, Q.; Cai, B.W.; Altan, O. Evolution of soil salinization under the background of landscape patterns in the irrigated northern slopes of Tianshan Mountains, Xinjiang, China. *Catena* **2021**, *206*, 105561. [[CrossRef](#)]
67. Chen, Y.; Li, Z.; Xu, J.; Shen, Y.; Xing, X.; Xie, T.; Li, Z.; Yang, L.; Xi, H.; Zhu, C.; et al. Changes and Protection Suggestions in Water Resources and Ecological Environment in Arid Region of Northwest China. *Bull. Chin. Acad. Sci.* **2023**, *38*, 385–393.

68. Jiang, F.-q.; Yu, Z.-y.; Zeng, D.-h.; Zhu, J.-j. The Three-North Shelter Forest Program needs ecological civilization. *Chin. J. Ecol.* **2009**, *28*, 1673–1678.
69. Guo, X.; Chang, Q.; Liu, X.; Bao, H.; Zhang, Y.; Tu, X.; Zhu, C.; Lv, C.; Zhang, Y. Multi-dimensional eco-land classification and management for implementing the ecological redline policy in China. *Land Use Policy* **2018**, *74*, 15–31. [[CrossRef](#)]
70. Tengberg, A.; Radstake, F.; Zhang, K.; Dunn, B. Scaling up of Sustainable Land Management in the Western People's Republic of China: Evaluation of a 10-Year Partnership. *Land Degrad. Dev.* **2016**, *27*, 134–144. [[CrossRef](#)]
71. Abulaiti, A.; Nurmemet, I.; Muhetaer, N.; Xiao, S.; Zhao, J. Monitoring of Soil Salinization in the Keriya Oasis Based on Deep Learning with PALSAR-2 and Landsat-8 Datasets. *Sustainability* **2022**, *14*, 2666. [[CrossRef](#)]
72. Du, B.; Cheng, Y.; Wu, L. Analysis of negative correlation between vegetation and soil salinization in Junggar Basin. *Acta Ecol. Sin.* **2021**, *41*, 9364–9376.
73. Yang, H.; Chen, Y.; Zhang, F. Evaluation of comprehensive improvement for mild and moderate soil salinization in arid zone. *PLoS ONE* **2019**, *14*, e0224790. [[CrossRef](#)]
74. Liang, Z.W.; Zou, T.; Liu, X.C.; Liu, G.Y.; Liu, Z. Collaborative operation and application influence of sprinkler drip irrigation: A systematic progress review. *Int. J. Agric. Biol. Eng.* **2023**, *16*, 12–27. [[CrossRef](#)]
75. Incrocci, L.; Malorgio, F.; Della Bartola, A.; Pardossi, A. The influence of drip irrigation or subirrigation on tomato grown in closed-loop substrate culture with saline water. *Sci. Hortic.* **2006**, *107*, 365–372. [[CrossRef](#)]
76. Ma, G.; Qu, Z.; Wang, L.; Jia, Y.; Liu, Z. Spatial variation characteristics of soil salinity and organic matter in typical demonstration area of Hetao irrigation area. *Soil Fertil. Sci. China* **2022**, 17–28. [[CrossRef](#)]
77. Su, Y.; Li, T.X.; Cheng, S.K.; Wang, X. Spatial distribution exploration and driving factor identification for soil salinisation based on geodetector models in coastal area. *Ecol. Eng.* **2020**, *156*, 105961. [[CrossRef](#)]
78. Akter, F.; Bishop, T.F.A.; Vervoort, W. Space-time modelling of groundwater level and salinity. *Sci. Total Environ.* **2021**, *776*, 145865. [[CrossRef](#)] [[PubMed](#)]
79. Liu, H.; Liao, T.K.; Wang, Y.; Qian, X.M.; Liu, X.C.; Li, C.M.; Li, S.W.; Guan, Z.L.; Zhu, L.J.; Zhou, X.Y.; et al. Fine-grained wetland classification for national wetland reserves using multi-source remote sensing data and Pixel Information Expert Engine (PIE-Engine). *Giscience Remote Sens.* **2023**, *60*, 2286746. [[CrossRef](#)]
80. Chen, Y.F.; Niu, Z.G.; Johnston, C.A.; Hu, S.J. A Unifying Approach to Classifying Wetlands in the Ontonagon River Basin, Michigan, Using Multi-temporal Landsat-8 OLI Imagery. *Can. J. Remote Sens.* **2018**, *44*, 373–389. [[CrossRef](#)]
81. He, Y.J.; Yin, H.Y.; Chen, Y.W.; Xiang, R.; Zhang, Z.T.; Chen, H.Y. Soil Salinity Estimation Based on Sentinel-1/2 Texture Features and Machine Learning. *IEEE Sens. J.* **2024**, *24*, 15302–15310. [[CrossRef](#)]
82. Sarkar, S.K.; Rudra, R.R.; Sohan, A.R.; Das, P.C.; Ekram, K.M.M.; Talukdar, S.; Rahman, A.; Alam, E.; Islam, M.K.; Islam, A. Coupling of machine learning and remote sensing for soil salinity mapping in coastal area of Bangladesh. *Sci. Rep.* **2023**, *13*, 17056. [[CrossRef](#)]
83. Wu, W.C.; Zucca, C.; Muhaimeed, A.S.; Al-Shafie, W.M.; Al-Quraishi, A.M.F.; Nangia, V.; Zhu, M.Q.; Liu, G.P. Soil salinity prediction and mapping by machine learning regression in Central Mesopotamia, Iraq. *Land Degrad. Dev.* **2018**, *29*, 4005–4014. [[CrossRef](#)]
84. Li, K.; Ding, J.; Han, L.; Ge, X.; Gu, Y.; Zhou, Q.; Lyu, Y. Digital mapping of soil salinization in a typical oasis based on PlanetScope images. *Arid Land Geogr.* **2023**, *46*, 1291–1302.
85. Tan, J.; Ding, J.; Han, L.; Ge, X.; Wang, X.; Wang, J.; Wang, R.; Qin, S.; Zhang, Z.; Li, Y. Exploring PlanetScope Satellite Capabilities for Soil Salinity Estimation and Mapping in Arid Regions Oases. *Remote Sens.* **2023**, *15*, 1066. [[CrossRef](#)]
86. Xiao, S.T.; Nurmemet, I.; Zhao, J. Soil salinity estimation based on machine learning using the GF-3 radar and Landsat-8 data in the Keriya Oasis, Southern Xinjiang, China. *Plant Soil* **2024**, *498*, 451–469. [[CrossRef](#)]
87. Mohamed, S.A.; Metwaly, M.M.; Metwalli, M.R.; AbdelRahman, M.A.E.; Badreldin, N. Integrating Active and Passive Remote Sensing Data for Mapping Soil Salinity Using Machine Learning and Feature Selection Approaches in Arid Regions. *Remote Sens.* **2023**, *15*, 1751. [[CrossRef](#)]
88. Yang, L.; Ren, J.; Wang, Y.; Zhang, J.; Wang, T.; Li, K. Soil Salinity Estimation Model in Juyanze Based on Multi-source Remote Sensing Data. *Trans. Chin. Soc. Agric. Mach.* **2022**, *53*, 226–235.
89. Jiang, Z.; Hao, Z.; Ding, J.; Miao, Z.; Zhang, Y.; Alimu, A.; Jin, X.; Cheng, H.; Ma, W. Weighted Variable Optimization-Based Method for Estimating Soil Salinity Using Multi-Source Remote Sensing Data: A Case Study in the Weiku Oasis, Xinjiang, China. *Remote Sens.* **2024**, *16*, 3145. [[CrossRef](#)]

**Disclaimer/Publisher's Note:** The statements, opinions and data contained in all publications are solely those of the individual author(s) and contributor(s) and not of MDPI and/or the editor(s). MDPI and/or the editor(s) disclaim responsibility for any injury to people or property resulting from any ideas, methods, instructions or products referred to in the content.